JGR Space Physics

RESEARCH ARTICLE
10.1029/2019JA027510

Dipole Tilt Effect on Magnetopause Reconnection and the Steady-State Magnetosphere-Ionosphere System: Global MHD Simulations

J. W. B. Eggington[1], J. P. Eastwood[1], L. Mejnertsen[1], R. T. Desai[1], and J. P. Chittenden[2]

[1]Space and Atmospheric Physics Group, Blackett Laboratory, Imperial College London, London, UK, [2]Plasma Physics Group, Blackett Laboratory, Imperial College London, London, UK

Key Points:
- The migration of the reconnection X line with dipole tilt angle is shown for angles up to 90°
- Magnetopause reconnection becomes less intense and the X line less steady at large dipole tilt angles
- The dipole tilt introduces a convection asymmetry driving stronger FAC in the sunward facing hemisphere

Supporting Information:
- Supporting Information S1
- Figure S1
- Figure S2
- Figure S3
- Figure S4
- Figure S5
- Figure S6
- Figure S7

Correspondence to:
J. W. B. Eggington,
j.eggington17@imperial.ac.uk

Citation:
Eggington, J. W. B., Eastwood, J. P., Mejnertsen, L., Desai, R. T., & Chittenden, J. P. (2020). Dipole tilt effect on magnetopause reconnection and the steady-state magnetosphere-ionosphere system: Global MHD simulations. *Journal of Geophysical Research: Space Physics*, *125*, e2019JA027510. https://doi.org/10.1029/2019JA027510

Received 8 OCT 2019
Accepted 19 MAY 2020
Accepted article online 19 JUN 2020

Abstract The Earth's dipole tilt angle changes both diurnally and seasonally and introduces numerous variabilities in the coupled magnetosphere-ionosphere system. By altering the location and intensity of magnetic reconnection, the dipole tilt influences convection on a global scale. However, due to the nonlinear nature of the system, various other effects like dipole rotation, varying interplanetary magnetic field (IMF) orientation, and nonuniform ionospheric conductance can smear tilt effects arising purely from changes in coupling with the solar wind. To elucidate the underlying tilt angle dependence, we perform magnetohydrodynamic (MHD) simulations of the steady-state magnetosphere-ionosphere system under purely southward IMF conditions for tilt angles from 0–90°. We identify the location of the magnetic separator in each case and find that an increasing tilt angle shifts the 3-D X line southward on the magnetopause due to changes in magnetic shear angle. The separator is highly unsteady above 50° tilt angle, characteristic of regular flux transfer event (FTE) generation on the magnetopause. The reconnection rate drops as the tilt angle becomes large, but remains continuous across the dayside such that the magnetosphere is open even for 90°. These trends map down to the ionosphere, with the polar cap contracting as the tilt angle increases, and region I field-aligned current (FAC) migrating to higher latitudes with changing morphology. The tilt introduces a north-south asymmetry in magnetospheric convection, thus driving more FAC in the Northern (sunward facing) hemisphere for large tilt angles than in the Southern independent of conductance. These results highlight the strong sensitivity to onset time in the potential impact of a severe space weather event.

Plain Language Summary The magnetic field of the Earth is tilted with respect to the Sun; as the planet orbits and rotates, the angle of this tilt changes. When the interplanetary magnetic field—which is carried by the solar wind—meets the Earth's magnetic field, a cavity is formed in the solar wind. Depending on the tilt angle, some mass and energy is able to penetrate into this cavity, affecting conditions in near-Earth space, in the upper atmosphere, and on the ground. To better understand how the tilt angle controls this, we perform computer simulations of the interaction between the solar wind and the Earth's magnetic field. We show that when the tilt angle is larger, less mass and energy can penetrate through, but the impact on one hemisphere of the Earth can be more severe and localized than on the other. This demonstrates that the potential impact of a solar storm for a given location on the Earth depends strongly on when the storm first hits.

1. Introduction

The interaction between the solar wind and the magnetosphere drives a highly complex dynamical system, affecting conditions in the near-space environment and on the ionosphere. At Earth, the dominant physical process behind this interaction is magnetic reconnection. Through reconnection, magnetic field which exists in different domains can merge, altering the magnetic topology and converting magnetic energy into kinetic and thermal energy in the local plasma. At the magnetopause, reconnection occurs between the planetary magnetic field and the interplanetary magnetic field (IMF) in the solar wind, opening “closed” magnetospheric field and driving large-scale convective flows (Dungey, 1961).

While magnetopause reconnection appears as a quasi-2-D process with a well-defined X line and inflow/outflow regions, the full 3-D nature of reconnection is much more complex, occurring predominantly along the magnetic separator: a continuous line along which differing magnetic topologies meet and which

is terminated by magnetic null points (where $|\mathbf{B}|=0$) (Dunlop, Zhang, Bogdanova, Lockwood, et al., 2011). The rate of reconnection at some point along this line is closely determined by the angle between the field either side the magnetopause, that is, the magnetic shear angle, and is maximized for the given local plasma conditions where the shear angle is 180°. One description which attempts to predict the X line location on the magnetopause is antiparallel reconnection, in which reconnection occurs where the shear angle is largest (Crooker, 1979). This angle depends on the relative orientation of the IMF and the planetary dipole axis; the angle that the latter makes with the Z axis of the Geocentric Solar Magnetic (GSM) coordinate system is the "dipole tilt angle" (denoted by μ) and varies annually between $\pm 34°$ (Hapgood, 1992). For purely southward IMF and a small tilt angle, antiparallel reconnection should occur anywhere along a line across the magnetic equator, and for purely northward IMF at high latitudes in the noon-midnight plane. Introducing an arbitrary and nonzero IMF B_y component splits the reconnection line at noon, with antiparallel regions in each of the dawn and dusk hemispheres.

However, in general, magnetic reconnection does not require antiparallel fields (e.g., reviews by Cassak & Fuselier, 2016; Eastwood et al., 2013; Hesse et al., 2011; Paschmann et al., 2013), leading to the concept of guide field, or component reconnection, where the out-of-plane magnetic field is nonzero at the X line (Gonzalez & Mozer, 1974; Sonnerup, 1974). This permits an extended continuous X line across the dayside magnetopause for nonsouthward IMF, which has been observed using multispacecraft observations (e.g., Dunlop, Zhang, Bogdanova, Trattner, et al., 2011). Various models have been developed to predict the orientation and location of the X line as a function of upstream conditions, in particular the magnetic field orientation in the magnetosheath (e.g., discussion by Komar et al., 2015), which have also been tested against observations (Souza et al., 2017; Walsh et al., 2017). Furthermore, Polar spacecraft data have shown that (except in cases where the IMF B_x is large) the reconnection line is continuous during southward IMF and generally follows the ridge of maximum magnetic shear, but does not necessarily cross the subsolar point (Trattner et al., 2007). This complication in the component description arises due to seasonal variations in dipole tilt angle, since the region of maximum shear shifts southward during northern summer and northward during northern winter. The maximum magnetic shear model has also been applied to observations from the Time History of Events and Macroscale Interactions during Substorms (THEMIS) mission (Trattner et al., 2012), showing this same seasonal dependence, and a similar effect was found by combining THEMIS and Cluster data (Zhu et al., 2015).

Magnetohydrodynamic (MHD) simulations have been used to explore the effect of dipole tilt angle on reconnection in more detail. The location of the separator has been shown for tilt angles between $-20°$ and $+20°$, showing the X line as continuous and shifting with tilt angle in the same fashion as described above (Hoilijoki et al., 2014). The inclusion of an IMF B_x component also contributes to this shift, as demonstrated in previous simulations (Peng et al., 2010). However, a recent survey of THEMIS data revealed that the seasonal (tilt angle) control of the X line location tends to dominate that of B_x (Hoshi et al., 2018). This seasonality may contribute to semiannual variations in geomagnetic activity (Russell & McPherron, 1973). Indeed, MHD simulations have shown that for increasing tilt angle and during southward IMF, the region of antiparallel magnetic field decreases in size (Russell et al., 2003) and changes location (Komar et al., 2015). While this may reduce the global rate of reconnection on the magnetopause, no such dependence has yet been quantified in simulations for the full range of tilt angles.

Additionally, this presumes that the reconnection location corresponds closely to these antiparallel regions, while in fact the full 3-D geometry and length of the X line will depend not only on the location and size of the antiparallel regions but also on the local plasma conditions and particular shape of the magnetopause for some given configuration. MHD simulations have shown that the magnetopause topology is highly sensitive to dipole tilt angle, with the location of the magnetopause nose (the point of first contact of the solar wind) shifting northward (southward) for a positive (negative) tilt angle, thus affecting the location of first contact with the solar wind and the predictions of component reconnection (Liu et al., 2012; Lu et al., 2013). Furthermore, observations have shown that the tilt introduces asymmetries in the bow shock (Jelínek et al., 2008; Lu, Zhou et al., 2019). Extending such a study beyond the terrestrial parameter range may reveal even more complex behavior.

In addition to altering the rate of open flux production, the tilt angle may introduce asymmetries in magnetospheric convection which would affect the global dynamics. Park et al. (2006) showed that

during southward IMF and for a static dipole with a 30° tilt angle, the dayside reconnection location (inferred by antiparallel regions) shifts to roughly follow the magnetic equator, while the nightside reconnection location follows the shift of the magnetotail current sheet. The latter is hinged by the magnetotail geometry toward the ecliptic plane, such that convection in the Northern Hemisphere is forced to follow a longer pathway than in the south. Similar hinging effects have been found in spacecraft data, showing a clear seasonal dependence (Xiao et al., 2016). Any such dynamical changes in the magnetosphere will also manifest in the ionospheric convection; due to its finite conductivity, the ionosphere acts like a resistor in a global electric circuit. Field-aligned currents are generated due to flow shear across the convecting field and are responsible for various space weather impacts, such as geomagnetically induced currents (GICs). Understanding the drivers for reconnection is important not only in predicting the state of the magnetosphere-ionosphere system but also in mitigating societal impacts (Eastwood et al., 2017).

Park et al. (2006) suggested that a north-south asymmetry in ionospheric cross-polar cap potential (CPCP, sometimes referred to as CPCP difference since it describes a voltage) develops since the convection electric field is stronger on average in the Northern Hemisphere. Similar asymmetries were also seen in simulations using duskward IMF with a nonzero dipole tilt angle (Park et al., 2010). Ridley et al. (2004) investigated the control of conductance in models on the magnetosphere-ionosphere system under southward IMF, showing that at solstice during northern summer the northern field-aligned currents are significantly stronger than at the south. This has similarly been shown in simulations of the IMF switching from northward to southward (Lu, Zhang, et al., 2019), which also found differences in the northern and southern polar cap sizes due to the dipole tilt angle having an asymmetric impact on the cusp in each hemisphere. However, the inclusion of nonuniform conductance (accounting for enhanced solar extreme ultraviolet (EUV) ionization in the sunlit hemisphere) has been shown to be largely responsible for disparities in northern and southern field-aligned currents (FAC) in simulations (Ridley, 2007). Simulating with a uniform conductance—and for the full range of tilt angles—would isolate the contribution of any convection asymmetries that arise purely due to changes in the location of reconnection.

Within observations there is no clear consensus on any north-south asymmetry in CPCP, with some studies finding larger values in both summer (e.g., Pettigrew et al., 2010) and winter (e.g., Zhang et al., 2007). Differences in observed FAC are more consistent, with data showing that the maximum summer FAC can be roughly twice the maximum winter FAC (Papitashvili et al., 2002; Wang et al., 2005). Recent AMPERE data even show stronger average region I FACs driven in the northern ionosphere independent of season (Coxon et al., 2016). Any such asymmetries are of consequence for the potential impact of a severe space weather event, since the onset time will closely determine which locations on the Earth experience the strongest enhancements in FAC.

It should be noted that seasonal effects (due to the inclination of the Earth's rotation axis to the ecliptic) contribute only 23.5° of the annual tilt angle variation, with the remaining ∼10° arising from the offset of the geomagnetic dipole to the rotation axis. Cnossen and Richmond (2012) explored the impact that more extreme offsets might have on ionospheric conditions, showing variations over 24-hr periods for tilt angles up to 60° at both solstice and equinox. While at equinox a trend of decreasing daily-average CPCP was seen for increasing tilt angle in both hemispheres, such a clear trend was not seen at solstice. Later simulations using the true offset showed that changes in solar wind coupling can account for up to 90% of CPCP variation and conductance effects as little as 10% (Cnossen, Wiltberger, & Ouellette, 2012). However, daily averaging will smear-out much of the magnetospheric response to dipole orientation, making it difficult to distinguish between driving factors.

Overall it is clear that the dipole tilt introduces significant asymmetries in the magnetosphere-ionosphere system, but the exact tilt angle dependence is not well understood. By eliminating various factors like dipole rotation and nonuniform conductance, and focusing on static, steady-state configurations, we can demonstrate with more clarity the fundamental impact of a varying tilt angle arising from only changes in magnetopause reconnection and magnetospheric convection. In fact, while the Earth's tilt angle variation is limited to a range of ±34° at present, this will not always be the case. The internal magnetic field is known to vary significantly over geological timescales, often undergoing full reversals every few hundred-thousand years (Gubbins, 2008). Additionally, between these dramatic reconfigurations there are periods of temporary

migration known as "geomagnetic excursions." Noticeable tilt angle variations can occur even on decadal timescales, with a total change of ~1° over the last half a century (Amit & Olson, 2008; Korte & Mandea, 2008). Hence, more severe dipole tilt configurations (i.e., beyond the present 34° tilt angle) could one day represent a realistic scenario for a severe space weather event.

Highly inclined dipoles are also a feature of interest outside of the terrestrial context. In particular, the dipole axes of Uranus and Neptune are offset by large angles to their rotation axes (by 60° and 47°, respectively) (Russell & Dougherty, 2010). Coupled with their severe obliquity to the ecliptic plane, these magnetospheres undergo significant reconfiguration both diurnally and seasonally as shown in both observations (e.g., Cowley, 2013) and simulations (e.g., Cao & Paty, 2017; Mejnertsen et al., 2016). More exotically, cases of tidally locked exoplanets and direct evidence of exoplanet magnetic fields suggest the possibility of magnetospheres that, as well as being highly inclined to the stellar wind, are locked-in to this extreme tilted configuration—though such a slow rotation rate might not support a strong planetary dynamo (Grießmeier et al., 2004). Thus, understanding the behavior of the magnetosphere-ionosphere system for larger tilt angles is important not only for revealing the key parameter dependencies of the terrestrial space environment but also in exploring the various cases which may indeed exist in nature.

In this study we investigate differences in the steady-state magnetosphere-ionosphere system for the full range of dipole tilt angles from 0° to 90°, in each case tilting the Northern Hemisphere to face sunward and keeping the dipole static. Changes in the location and intensity of dayside magnetopause reconnection are investigated in each case, to reveal the key determining factors in the case of southward IMF. We thus explore how changes in coupling with the solar wind affect magnetospheric dynamics, and the asymmetries that develop in the convection due to the tilt angle effects in more detail than has been shown before. Finally, these results are used to explain the various impacts on ionospheric conditions, revealing the key role of tilt angle on modulating the location, strength, and morphology of the region I current system, and thus the importance of this parameter in determining potential impacts as a function of onset time for a given severe space weather event.

2. Methodology

2.1. The Gorgon MHD Code

In this study we use the Gorgon 3-D MHD code (Ciardi et al., 2007), which solves the resistive semiconservative MHD equations via a fully explicit, Eulerian formulation. Due to its heritage in high-energy laboratory plasmas, certain treatments of the plasma are unique compared to other magnetospheric codes. Gorgon utilizes separate ion and electron energy equations, which allows each species to be out of thermal equilibrium. Furthermore, the code utilizes a vector potential representation of the magnetic induction equation; via the use of a staggered grid this leads to a divergence-free magnetic field up to machine precision and removes the need for various computationally expensive divergence cleaning algorithms. As in many other magnetospheric codes we employ a split dipole magnetic field—that is, $\mathbf{B}=\mathbf{B}_0+\mathbf{B}_1$ where $\mathbf{B}_0$ is the curl-free (dipole) component—which reduces discretization errors close to the Earth (Tanaka, 1994). While the code can account for various collisional plasma phenomena, the terms in the MHD equations which control these are generally set to be negligibly small or zero, enforcing a collisionless regime when modeling space plasmas.

Previous studies using Gorgon include modeling Neptune's magnetosphere (Mejnertsen et al., 2016) and the motion of the Earth's bow shock in response to a variable solar wind (Mejnertsen et al., 2018). In these studies the inner region was treated as a vacuum containing a dipole source, where the magnetic field was propagated via the vacuum wave equation; by allowing the field to vary on the inner boundary, it behaved as resistive surface with an effective finite conductance. However, in order to capture the coupling with the ionosphere, we have extended the model to adopt a more standard inner boundary treatment. In this approach the plasma flow at the inner boundary is set according to the ionospheric convection electric field by solving the continuity equation on a model thin-shell ionosphere (Eggington et al., 2018). FACs are mapped-down from a fixed radius onto the ionospheric grid, and the resultant electric potential is mapped-out to the cells within the inner boundary to calculate the $E\times B$ drift, whereby it feeds through to the rest of the simulation.

This potential is set to be zero at the lower-latitude boundary of the mapped region on the ionosphere. The ionospheric convection is always perpendicular to the magnetic field; since we set the parallel velocity to be zero, there is thus no flow at the magnetic equator at the inner boundary. By use of a fixed mass density in the inner region, any mass entering at higher latitudes is effectively removed, and the MHD equations are not solved. While the nondipolar magnetic field component $\mathbf{B}_1$ is allowed to float within the inner region, it is generally negligible; we can thus assume a perfectly dipolar field here, allowing the use of dipole coordinates to map the relevant quantities (Goodman, 1995).

2.2. Simulation Setup

Our simulations employ a domain of dimensions X=(−30,90) R_E, Y=(−40,40) R_E, Z=(−40,40) R_E, and a uniform, Cartesian grid of resolution 0.5 R_E. Note that this coordinate system essentially corresponds to GSM but is positive in the antisunward direction, that is, $(X,Y,Z)=(-X_{GSM},-Y_{GSM},Z_{GSM})$. The solar wind propagates in from the sunward edge of the box (at $X=-30R_E$), and the remaining outer boundaries apply free-flow conditions. The dipole is located at the origin, at the center of a spherical inner boundary of radius 4 R_E at which the number density and ion/electron temperature are fixed to n=370 cm^{-3} and $T_{i,e}$=0.1 eV, respectively.

In each of our simulations, we initialize the magnetosphere with 4 hr of purely southward IMF (B_z=−2 nT) driving using a synthetic, steady solar wind of velocity v_x=400 km s^{-1}, number density n=5 cm^{-3} and ion/electron temperature $T_{i,e}$=5 eV. This gives time for the magnetosphere to enter a quasi-steady state, and for the CPCP to approach a maximum value. We have performed this same simulation for a series of dipole tilt angles from 0–90° in steps of 10°, whereby a positive dipole tilt angle denotes the northern magnetic pole (i.e., at positive Z in GSM coordinates) pointing toward the Sun.

In all our simulations we take a common approach of using a uniform Pedersen conductance of 10 mho and zero Hall conductance (see Merkin & Lyon, 2010), meaning we do not include the effects of EUV ionization and auroral precipitation. In reality these will be altered by the dipole tilt angle due to changes in the solar zenith angle and would create further asymmetries in the system. Furthermore, it has been shown that changes in ionospheric conductance can impart changes in the reconnection rate in models by affecting the magnetopause geometry (Merkin et al., 2003). However, coupled with the already complex geometric effects of dipole tilt, the exact effect of a changing conductance profile on the global dynamics is hard to diagnose separately, and is outside the scope of this study.

2.3. Numerical Resistivity

While reconnection strictly should not occur in collisionless MHD (as an electrical resistivity is required to allow diffusion of the magnetic field), one consequence of solving the MHD equations on a discrete grid is that the field will numerically diffuse to an extent that is determined by the coarseness of the grid and the numerics of the code. Reconnection in simulations will therefore occur numerically wherever there is a sufficiently strong current layer, its rate dependent on the grid resolution chosen. Ridley et al. (2010) showed that an increased resolution on the dayside magnetopause decreases the reconnection rate, and thus the CPCP. Conversely, a finer resolution in the inner magnetosphere acts to increase the CPCP, due to reduced discretization errors in the magnetic field. The use of a uniform grid resolution in this study ensures no priori assumption is required about where numerical reconnection is likely to occur on the magnetopause, since the grid effects will be self-consistent across all tilt angles.

One way to more closely control reconnection in simulations is by artificially setting either a uniform or anomalous resistivity, independent of the numerics. Various other studies exploring dayside reconnection in MHD simulations have employed such resistivity models throughout the entire simulation domain, with values often much greater than the actual resistivity in the magnetosphere. This acts to smooth the magnetopause current sheet, making it more stable to reconnection and reducing the occurrence of flux transfer events (FTEs), such that reconnection occurs steadily along a single X line. Raeder (2006) showed that for a tilted dipole, FTEs are more likely to occur in simulations due to flux piling up at the dayside magnetopause, provided the grid resolution is sufficiently high (or else strong numerical diffusion prevents sufficient flux pileup). However, Dorelli and Bhattacharjee (2009) showed that FTE generation can still occur with zero tilt angle, suggesting FTE generation may be more closely related to movement of the flow stagnation point away from the magnetic separator. Glocer et al. (2016) traced magnetic separators in simulations for

cases of small and large uniform resistivity, showing splitting of the separator into multiple X lines due to FTE occurrence where the resistivity was small.

While our resolution of 0.5 R_E results in a relatively coarse magnetopause, it ensures that (at least for the smaller tilt angle cases) FTEs are less likely to develop. Furthermore, it becomes more straightforward to quantify the reconnection rate where there is a single well-defined X line. Setting a large uniform resistivity or current-dependent anomalous resistivity (e.g., Uzdensky, 2003) would also aid in this. However, in our runs reconnection is essentially entirely driven by numerical diffusion. While the Gorgon code contains a Spitzer resistivity, analysis shows that it plays a negligible role at the magnetopause and is several orders of magnitude below those required to compete with numerical effects.

3. Simulation Results

3.1. Magnetospheric Dynamics

To explore how the dipole tilt angle affects the field topology in the magnetosphere, we focus on the example cases of 0°, 30°, and 90°. We have chosen these as they represent the symmetric (untilted) case, the realistic extreme case at present (i.e., the approximate tilt angle at noon in northern summer), and the limit of the parameter space. Figure 1 shows plots of the current density and open magnetic field lines in the magnetosphere in the *X*-*Z* plane for each of these tilt angles, shown after 4 hr of simulation (see supporting information for other angles). The location of the magnetopause and approximate dayside and nightside reconnection sites are indicated. The magnetopause is defined as the boundary at which there is minimum solar wind entry into the magnetosphere, similar to the method of Palmroth et al. (2003). We launch a large number of flow streamlines (~40,000) from the sunward edge of the simulation box and identify the boundary about which they are diverted by finding voids (minima) in the streamline density (Mejnertsen, 2018). These voids are binned onto a parabolic grid, as this effectively captures the spherical dayside and cylindrical nightside geometries. The location of the reconnection sites are simply approximated by inspection.

For 0° tilt angle, the dayside reconnection site, nightside reconnection site, and magnetotail current sheet all lie in the equatorial plane. For 30°, the dayside reconnection site is found to have moved southward, roughly aligned to the magnetic equator on the magnetopause. Notably, the magnetotail current sheet does not lie in the same plane as this point and is hinged downward due to the magnetotail geometry being dominated by the solar wind pressure at large downstream distances, as found in other simulations (Park et al., 2006). This appears to offset the tail reconnection site, with the closed field lines tilted away from the magnetic equator, the implication being that field lines opened in the Northern Hemisphere must cover a longer convection path before again reconnecting on the nightside. In a steady configuration where northern and southern magnetic field lines open and close at equal rates (and each hemisphere contains equal amounts of open flux), the result will be a stronger convection electric field on average in the Northern Hemisphere than the Southern.

In the more extreme 90° case, the dayside reconnection region has moved yet further southward on the magnetopause, and the same hinging effect is present at the tail reconnection site, with the current sheet slightly northward of the 30° configuration. However, the dayside reconnection site is no longer located close to the magnetic equator, but lies roughly half-way down from the subsolar magnetopause. Extending the tilt angle range to more extreme values has thus revealed a more complex dependence than is initially apparent.

Another key effect is in the changing size and shape of the magnetopause and bow shock, with the tail magnetopause shrinking in its *Z* dimension and the subsolar bow shock moving upstream with increasing tilt angle. The magnetopause nose is shifted southward for 30°; at 90° the nose has returned to the subsolar point, and the dayside magnetopause appears flatter and larger overall than for 0°. This is a result of the dipole field strength being greatest at the magnetic pole, which for 90° directly faces the solar wind. This pole-on configuration has further consequences for the newly-reconnected dayside magnetic field, as the reconnection outflow south of the subsolar magnetopause will be largely in the z direction. For newly opened magnetospheric field lines connected to the North Pole, the resulting convection will be mostly perpendicular to the magnetic field in the subsolar region, generating a strong electric field here. If the electric field is stronger on the dayside than the nightside, this may influence the region I FAC toward noon on the

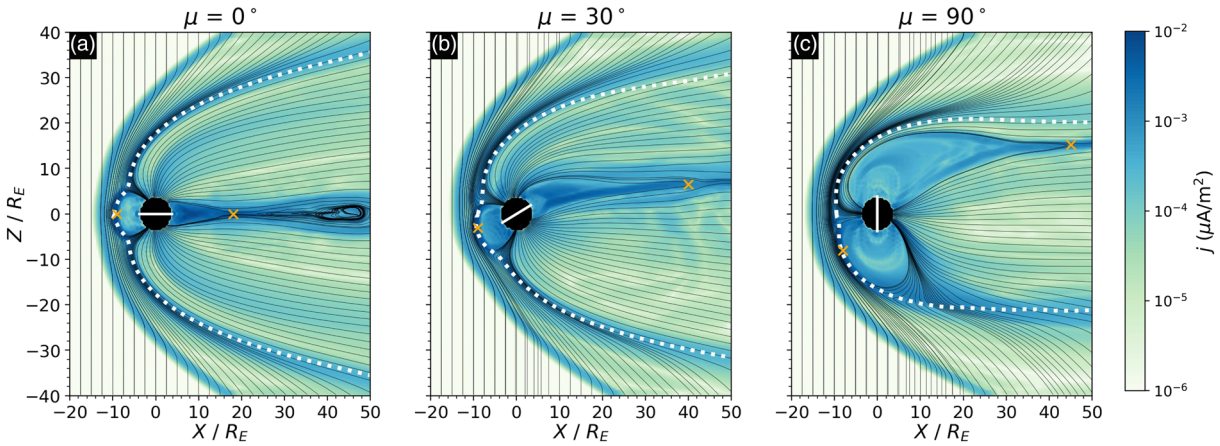

Figure 1. The current density j and open magnetic field lines (in black) in the noon-midnight plane for (a) 0°, (b) 30°, and (c) 90° dipole tilt angles, shown after 4 hr of simulation. The solid white line denotes the magnetic equator, the dotted white line represents the magnetopause, and the orange crosses mark the approximate location of the reconnection site. Note that the density of field lines in these plots is not exactly proportional to the local magnetic field strength.

ionosphere, since footpoints here connect to regions in the magnetosphere with stronger flow shear (see section 3.3).

The closed field regions grow in size on both the dayside and nightside as the tilt angle increases, due to a reduction in open flux content in the magnetosphere (see Figure S2 in the supporting information). The consequences should thus be reduced geomagnetic activity and smaller ionospheric polar caps, supporting the notion that these are seasonally modulated due to changing tilt angle. The reduced open flux content suggests an associated drop in the reconnection voltage, despite the upstream solar wind conditions being identical in each case. Notably, from the traced field lines for 0° we see a plasmoid being ejected downtail from the near-Earth neutral line, suggesting that (numerical) reconnection in the magnetotail is bursty in this case. As a result the magnetosphere can only be quasi-steady, to an extent determined by the variability in dayside and nightside reconnection. However, whether reconnection is more or less bursty for a given tilt angle is not clear from viewing the global configuration. To understand this in more detail, we now look more closely at the nature of dayside reconnection and attempt to quantify how the rate of flux transfer varies with tilt angle.

3.2. Magnetopause Reconnection

3.2.1. Dayside Topology and FTE Generation

The motion of the reconnection site for a varying tilt angle arises due to changes in the magnetic topology at the dayside magnetopause, since the X line is located at the intersection of magnetic domains. These domains can be identified in the simulation by tracing field lines in both directions from various points in the magnetosphere. Where the field lines terminate defines the magnetic connectivity of these points, that is, "solar wind," "closed," "north open," or "south open." In the solar wind case, both ends exit the simulation box; in the closed case, both ends terminate at the dipole source; in the north/south open cases, one end exits the box and the other terminates at the North/South Pole of the Earth. The field line may fail to terminate; this either indicates a magnetic island or can occur spuriously due to interpolation errors. Structures of this connectivity imply FTE generation, and thus we label this domain as "FTE". Figure 2 shows magnetic connectivity and flow streamlines around the dayside magnetopause in the noon-midnight meridian plane for each tilt angle at a single point in time, with each domain colored according to the key.

At 0° we see evidence of an FTE being formed around the subsolar region. The steady X line is diverted into two separate X lines at $\pm 2\ R_E$, and the flow streamlines terminate within this structure, suggesting that the flow may be vortical inside the FTE. This is consistent with the findings of Dorelli and Bhattacharjee (2009), in that dipole tilt is not required in the formation of an FTE even if there is a tilt angle dependence to their formation rate. In this case, however, the FTE may be a result of significant erosion of the subsolar magnetopause due to the large reconnection rate, making the current sheet thin and less stable (exacerbated by the coarse grid resolution). Indeed, from 10° to 40° there are no FTEs around the reconnection region at this specific point in time, implying that reconnection is generally more steady for the smaller tilt angles. This

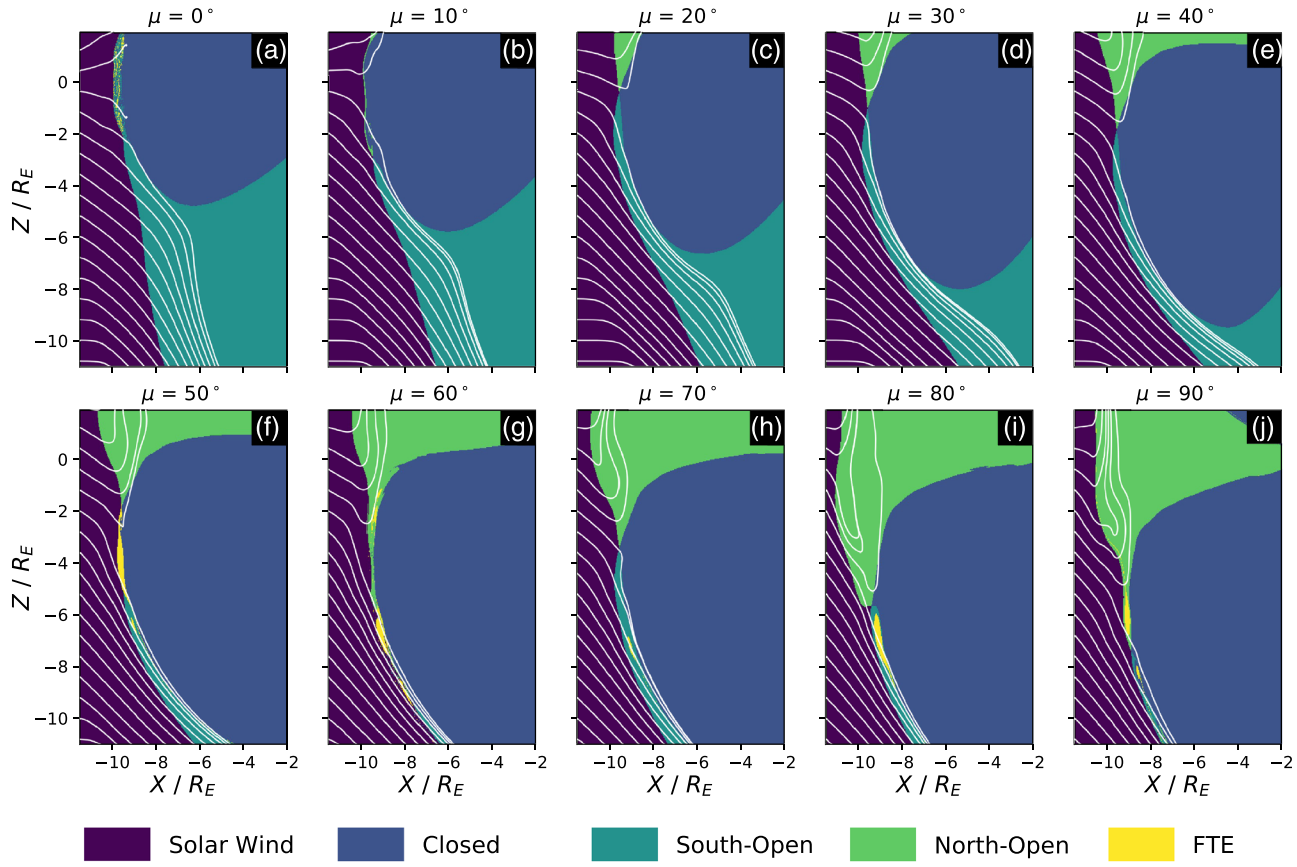

Figure 2. Magnetic topology at the dayside in the noon-midnight meridian plane for successive dipole tilt angles (a–j) after 13,800 s of simulation. Shown as white lines are streamlines calculated from the bulk velocity projected onto the *X*-*Z* plane.

reflects the fact that the 0° case is unique in that reconnection is completely antiparallel along the equatorial plane, whereas the antisymmetry between the IMF and magnetospheric field breaks down the moment a tilt is introduced.

For tilt angles of 50° and above, there is persistent evidence of FTEs on the magnetopause, though not necessarily located at the separator. This indicates that steadiness of magnetopause reconnection may depend on the tilt angle, in agreement with Raeder (2006), and that the separator location becomes more time dependent with increasing tilt angle. For these large tilt angles, the flow streamlines are diverted far from the subsolar region and can be almost parallel to the magnetopause at the separator location. While the stagnation point (where the streamlines diverge) is coincident with the steady X line for 20–40° tilt angles, it appears to be the source region for FTEs at large tilt angles. This is consistent with the FTE generation mechanism of Dorelli and Bhattacharjee (2009), whereby diversion of the magnetosheath flow away from the separator renders the flow unstable.

Thus, from the perspective of this 2-D projection, the tilt angle dependence in FTE occurrence may be due to the independent motions of the flow stagnation point and the steady X point with an increasing tilt angle. Nonetheless, this view only represents a single snapshot in time, while FTEs are an inherently transient phenomenon. Furthermore, our understanding of these structures is limited within this 2-D view, since the global 3-D X line configuration may be much more complex. To determine the relative stability of the separator and the extent of its deviation for different tilt angles, we must trace out its location over a long time period and thus examine its full 3-D motion.

3.2.2. Location of the X Line

Since reconnection predominantly occurs along the magnetic separator—which demarcates different magnetic domains—locating it does not require any prior assumption about whether reconnection is of

antiparallel or component type. To trace out its location in Gorgon, we adopt an approach derived from that of Komar et al. (2013). Magnetic null points (which terminate each end of the separator) are found using the method of Haynes and Parnell (2007), that is, we search for all grid cells containing reversals in each component of **B** and perform a trilinear interpolation to obtain subgrid coordinates.

For a given IMF clock angle, the terminating nulls at dawn and dusk can be selected by finding those closest to the vacuum superposition solutions (Yeh, 1976); this is nontrivial in the case of a dipole tilt or nonzero B_x, however, since the dipole axis and IMF cannot be treated as coplanar. Since we are driving with due southward IMF, there are infinite numbers of nulls in the equatorial plane for the 0° tilt angle case; for small tilt angles the null locations remain close to those in the 0° case. For larger tilt angles ($\gtrsim 30°$) the number of dayside nulls decreases dramatically and regular FTE generation leads to splitting of the separator into multiple X lines. This forms additional nulls around noon; as a general solution for all tilt angles, we thus select the dayside nulls closest to dawn and dusk, and trace from these. If the nulls in question do not lie along the terminator plane, we trace in both directions to terminate the separator where X=0, so that the entire dayside magnetopause is covered and the length of the separator is independent of the choice of nulls. Where there are multiple X lines formed, we simply allow the trace to follow only the one which is the least diverted from the steady X line. While tracing all of them is possible, these are only transient features that do not represent the average location of the separator and are not always well resolved with a coarse grid at the magnetopause.

To locate the separator about a chosen null point, we draw a hemispheric grid (oriented sunward) and trace magnetic field lines in both directions from each grid point to determine the magnetic connectivity. These hemispheres are of arbitrary size and resolution; for most of our traces we have used radii of 1 R_E and 50×50 grids. From these connectivities we construct a map of the magnetic domains about the vicinity of the null. We then employ image processing algorithms using the Python scikit-image package (van der Walt et al., 2014) to identify where the four domains converge, which defines the location of the separator on this grid. Using edge detection the boundaries of the connectivity structures (e.g., the closed region) are identified and uniquely labeled by which domains lie on either side. We sample through the grid and count how many such edges lie within a given region; the sample area that contains all four edges of the half-open domains is determined to contain the separator. We then draw a line straddling this sample area and interpolate along it to find the exact location of the convergence point. A new hemisphere is then drawn around this point, and the process is repeated until the opposite null point is reached (see supporting information for a schematic of this process).

We perform our trace in 5-min intervals for the final 30 min of the simulation and calculate the average separator location over this period, which should smooth-out transient changes in its configuration. This is done by interpolating the traced separators onto fixed, regularly spaced Y coordinates and taking the time-average of the resulting X and Z coordinates (see Text S1 of supporting information). Figure 3 shows the resulting magnetic separators for each tilt angle. In panel (a) we have also displayed the range in traced positions across the magnetopause in each case.

For 0°, the average separator lies roughly along the equatorial plane, deviating slightly at the subsolar point by about 1 R_E. For 10°, the terminating points of the separator have moved southward of their original locations, whereas in the subsolar region there is a large southward deviation, consistent with the observed topology in Figure 2b. For 20° to 60° this deviation is not seen, and the separators are shifted more weakly at the subsolar magnetopause than at the flanks. We note the similarities in this trend to the results found by Hoilijoki et al. (2014) up to 20°; our results show that this still holds for larger tilt angles. At 70° we see that the separator suddenly shifts more strongly at noon, creating a flatter average profile. At 80° and 90°, it continues to migrate southward at the flanks, but is deviated northward at noon, creating a narrow profile that increases the effective length of the X line. In general, the location of the dawn and dusk terminating points are shifted southward (in Z) and earthward (in Y) in a consistent manner, but it is the central portions that show a complex tilt angle dependence.

In the purely antiparallel case of 0°, there is a range of deviation of up to 1 R_E in the separator location over this interval, largest at noon. There is less deviation at 10°, and it remains relatively stable across its extent (with more motion at the flanks) up to 50°. However, the separator becomes significantly more time dependent from 60° onward, varying most at 70° by $\pm 3\,R_E$ over the 30-min interval. This is consistent with the

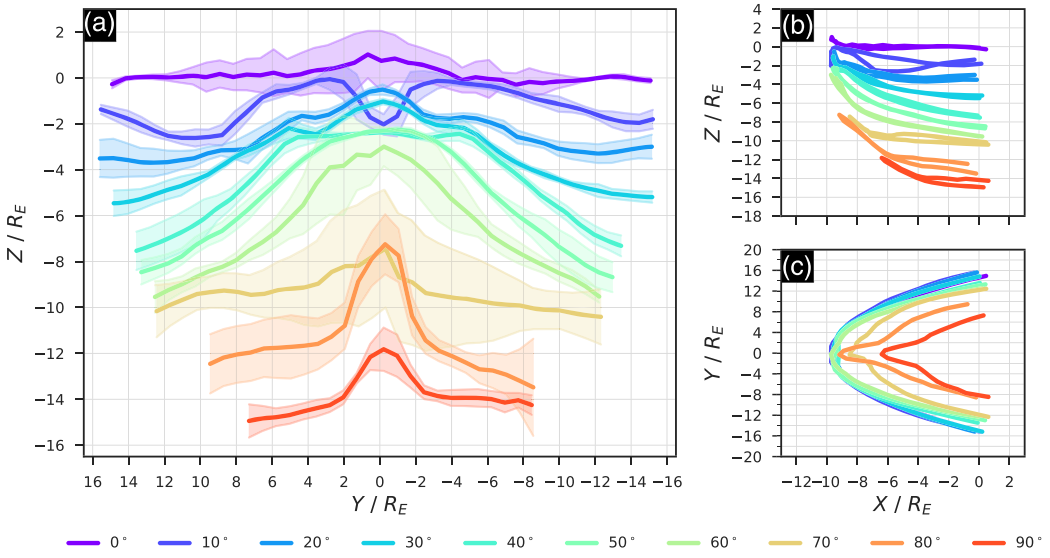

Figure 3. Traced magnetic separators at the dayside magnetopause for different dipole tilt angles, plotted in the *Y*-*Z* (a), *X*-*Z* (b), and *X*-*Y* (c) planes. Shown is the average location of the separator over the last 30 min of simulation, with the shaded regions representing 1 standard deviation in the *Z* direction.

observed prevalence of FTE generation for large tilt angles in Figure 2, which will significantly alter the dayside topology over short timescales. Overall, though the X line does not appear perfectly steady for any tilt angle, the degree to which it is stable appears to depend closely on the tilt angle.

To help explain the southward migration of the separator, Figure 4 shows the magnetic shear angle on the dayside magnetopause for 0°, 30°, and 90° tilt angles (see supporting information for other angles). For each set of magnetopause coordinates, we calculate surface normals using a procedure similar to that described by Komar et al. (2015), based on the method of Hoppe et al. (1992). The magnetic field is sampled either side of the boundary, stepping perpendicularly from the magnetopause coordinates, and the shear angle is calculated as the angle between the sampled fields. In the 0° case the separator can be seen to follow the region of antiparallel field, which covers the entire equatorial plane. For 30° this region has shrunk in size, and the separator is draped southward at the flanks toward where the shear is largest. For 90° the antiparallel region is reduced to essentially a single point about which the separator is approximately hinged. This suggests that, at least for purely southward IMF, the separator tends to reconfigure with tilt angle so as to maximize the shear angle along its extent, though can deviate around the subsolar region. This is consistent with the findings of Komar et al. (2015) for a 15° tilt angle, where the maximum magnetic shear model provided the most accurate prediction of X line location out of several tested models for southward IMF. However, we note that unlike in the present study the IMF used in their simulations was not purely southward, that is, it was southward oriented with a nonzero B_y.

Nonetheless, the separator geometry alone does not reveal information about the location or intensity of reconnection itself. To infer this, we calculate the electric field parallel to the separator along its full extent, which provides the local reconnection rate. Figure 5 shows the result for each tilt angle, time-averaged over the final 30 min and plotted on the average separator locations to give the typical intensity profile (see TextS2 of the supporting information). For 0–50°, the electric field intensity is focused around the central point, while it becomes much weaker for 60° and above. Where the separator is strongly deviated around noon (most notably at 10° and 80°), the electric field appears to drop, as was found by Glocer et al. (2016) during FTE generation. We note that for 0–30° tilt angles (where the separator crosses close to the Sun-Earth line) the enhanced reconnection rate around the subsolar region would yield a view consistent with component reconnection if measured locally. However, this electric field is nonzero elsewhere along the separator, which itself extends far away from the subsolar point. Similarly, the electric field is nonzero in regions of small magnetic shear for both 30° and 90°—in contrast to the predictions of antiparallel reconnection. Furthermore, while for 0° and 90° it reaches a maximum where the shear is largest, for the 30° case this

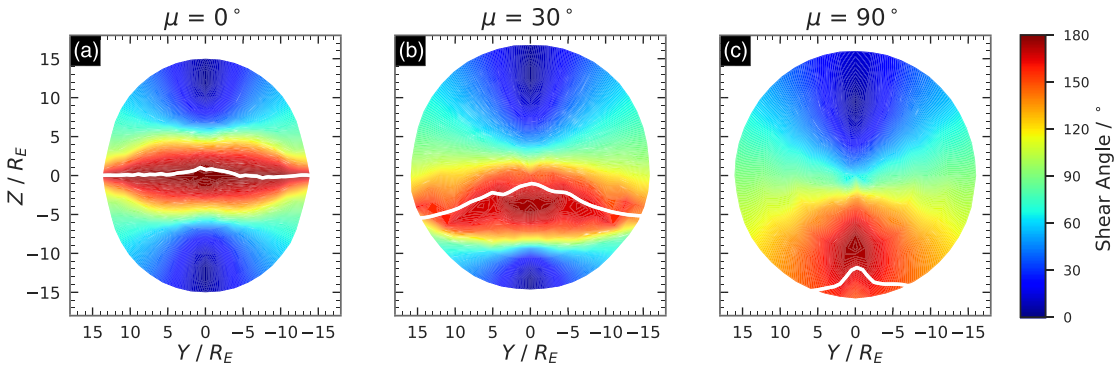

Figure 4. The magnetic shear angle on the dayside magnetopause for (a) 0°, (b) 30°, and (c) 90° dipole tilt angles, shown here in the *Y-Z* plane after 4 hr of simulation. The white lines are the average locations of the separator over the final 30 min, as shown in Figure 3.

occurs just northward of the region of maximum shear. As pointed out by Glocer et al. (2016), these paradigms may only present a local perspective of 3-D dayside reconnection and could lend to misleading conclusions if applied to a global context such at that shown here.

Integrating the parallel electric field over the length of the separator provides the dayside reconnection voltage, that is, the global rate of flux transfer into the magnetosphere. Figure 6a shows the result of calculating this for the traced separators (see Text S2 of the supporting information). From 10° onward the overall trend is that the average reconnection voltage decreases with increasing tilt angle for steady southward IMF. However, the calculated voltage is 15 kV lower at 0° than at 10°, despite the fact there is a greater open flux content at 0° during this interval (0.93 GWb in the Northern Hemisphere versus 0.84 GWb for 10°, see Figure S2 in the supporting information). This may imply that the dayside and nightside reconnection rates are not perfectly in balance, consistent with the formation of a plasmoid in Figure 1a. Additional complex

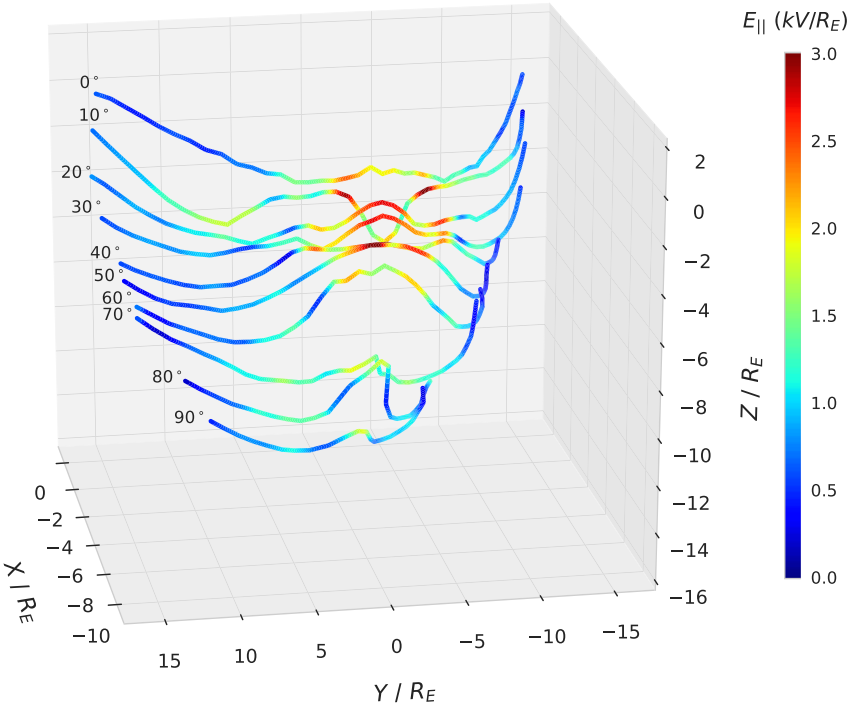

Figure 5. The electric field parallel to the magnetic separator for successive dipole tilt angles, averaged over the final 30 min of simulation.

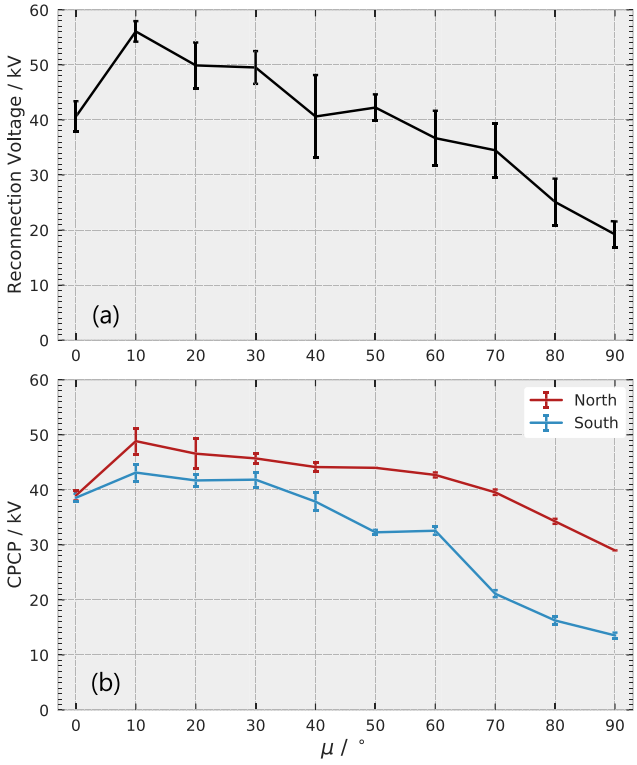

Figure 6. The dayside reconnection rate (a) integrated along the traced separators, and the ionospheric cross-polar cap potential (CPCP) (b) at each hemisphere for successive dipole tilt angles averaged over the final 30 min of simulation, with error bars representing 1 standard deviation.

magnetotail dynamics may therefore be required to explain the greater flux content in the purely antiparallel 0° case, and we reserve this for future study.

For all tilt angles the reconnection voltage is strongly time dependent—most notably at 40° where it varies by ±7 kV over this interval. Note that although we have not traced out all X lines where multiple were formed, the local reconnection rate tends to drop in the vicinity of the FTEs that they flank. Furthermore, Glocer et al. (2016) found that the calculated reconnection voltage was the same regardless of which separator branch was traced in their simulations, and so tracing other branches should not significantly affect our calculations. The shorter timescale behavior seen in the reconnection voltage should average out to achieve the global quasi-steady state, since the total flux is the time integral of the reconnection rate. The polar caps should therefore shrink with increasing tilt angle due to reduced open flux content, altering the location of ionospheric region I currents. Additional changes in the currents such as emerging north-south asymmetries may also lead to a more complex tilt angle dependence, which we now investigate.

3.3. Coupling With the Ionosphere

To explore how the tilt angle effects manifest in the ionosphere, we first examine the polar caps in more detail. In ideal MHD ($\mathbf{E}=-\mathbf{v}\times\mathbf{B}$) and in steady state ($\partial\mathbf{B}/\partial t=0$), the parallel electric field $E_{||}$ along magnetic field lines is zero. Thus, the electrostatic potential on closed field lines should be identical at conjugate north/south ionospheric footpoints (Hesse, 1997), and the reconnection voltage should map down as the CPCP. Figure 6b shows the CPCP at north and south for each tilt angle. On both hemispheres the overall trend in the CPCP matches that in the reconnection voltage, as expected.

The northern CPCP is generally comparable to the reconnection voltage, with some potential drop seen in each case. At the south, there is a larger drop in CPCP with growing tilt angle, introducing a north-south asymmetry that becomes significant at large tilt angles. Thus, the breaking of a global north-south symmetry in the magnetosphere also breaks the symmetry in the simulated north/south CPCPs, even with a uniform conductance profile, as suggested by Park et al. (2006) for a 30° tilt angle. This may arise since the constraint of matching potentials does not apply to open field lines (as these only map to one hemisphere), such that north-south asymmetries can arise in the potential and FAC due to asymmetries in the convection electric field in the magnetosphere. The disparity in CPCPs suggests that the FAC may differ significantly on each hemisphere at large tilt angles, even though the open-closed boundary (OCB) which encloses the polar caps should contain the same amount of flux in steady state and be of similar size. The region I current system is generated along this boundary due to flow shear (Cowley, 2000), and thus any flow asymmetries on open field lines will give rise to asymmetries in the FAC, introducing a hemispheric and local-time dependence in auroral oval latitude.

Figure 7 shows the ionospheric FAC profiles at north and south after 4 hr, with the OCB indicated. Once again we focus on 0°, 30°, and 90° as our example cases (see supporting information for other angles). For 0° the northern and southern conditions match, with the OCB sitting at 5° higher in latitude on the dayside such that the polar cap is shifted slightly to the nightside. The FAC profiles extend to noon, but are negligible at midnight. For the 30° tilt angle the polar caps have shrunk in size, and the northern OCB has shifted sunward such that it is now roughly centered between day and night. The northern FAC profile is broadened on the dayside, where the two bands of region I current reach maximum amplitudes. In the south this day/night asymmetry is not seen, and though region I currents reach slightly larger maximum values than in the north, they are thinner than in the 0° case and the total upward field-aligned current (TFAC) is now lower. For 90° the polar caps are now considerably smaller, bulging on the dayside in the north and showing more day-night symmetry in the south, continuing the trend of a sunward shift in OCB location in the north

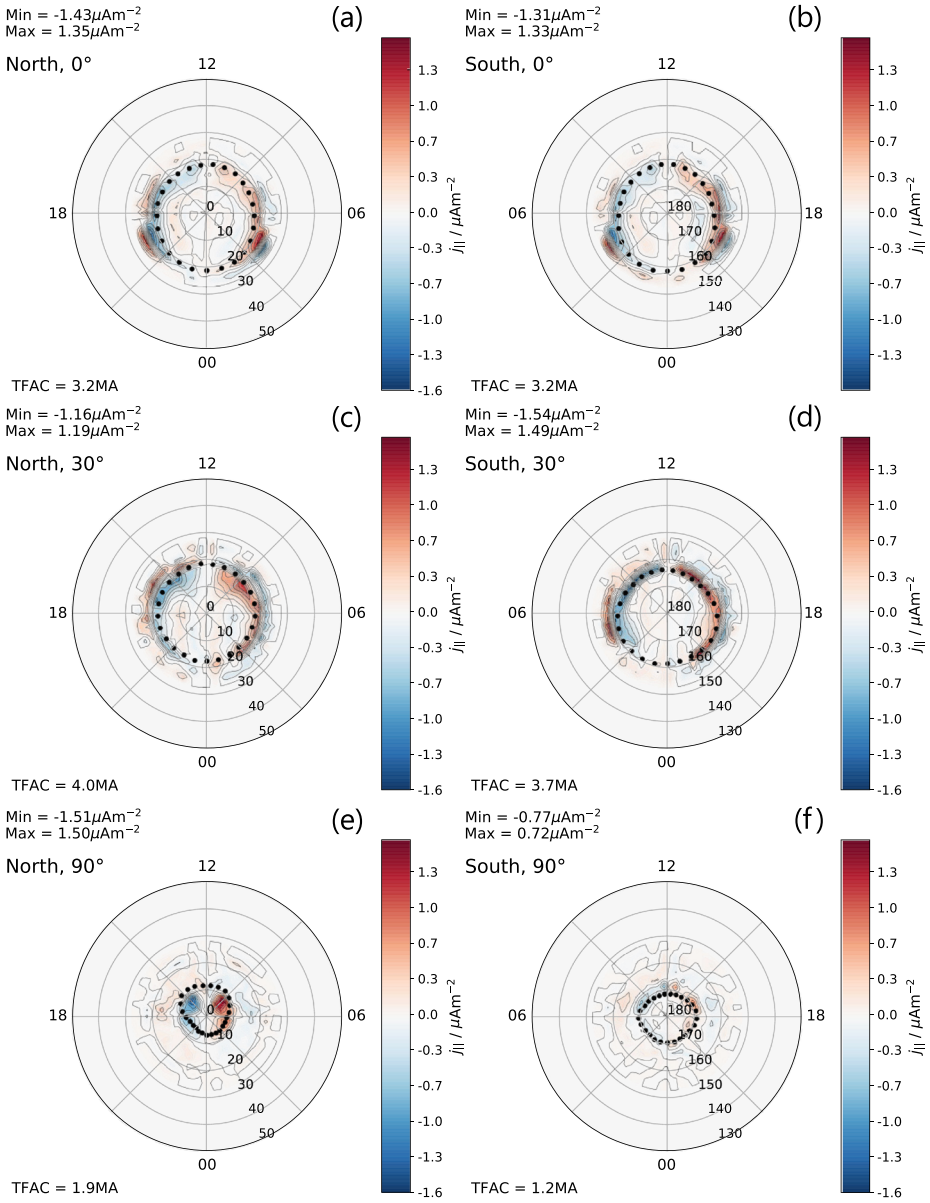

Figure 7. Field-aligned current $j_{||}$ at the northern (a, c, e) and southern (b, d, f) ionosphere after 4 hr of simulation for 0° (a, b), 30° (c, d), and 90° (e, f) dipole tilt angles. The dotted black lines mark the location of the open-closed boundary. The corresponding minimum/maximum FAC and TFAC is shown in each case.

with growing tilt angle. The result is a strongly localized region I current system with a much lower TFAC on both hemispheres. However, in the north the maximum FAC value is still comparable to the 0° case, and is clearly offset toward the dayside. At the south a slight dayside bias is seen, but this is much less significant than in the north and the currents are approximately half as intense.

Thus, as the tilt angle increases, a growing north-south asymmetry in each of the FAC, CPCP, and OCB emerges, despite our use of a uniform conductance profile. This asymmetry must therefore originate in the convection electric field itself; to explain this, we refer back to Figure 1 and our findings in section 3.1 , that is, that the convection path length for northern open field lines becomes longer than the southern field lines as the tilt angle increases. To sustain steady state, faster flows in the Northern Hemisphere—especially at the dayside where newly reconnected field flows strongly perpendicular to the polar cap surface—must thus drive stronger currents than in the south, and with an increasing bias toward noon.

4. Discussion and Conclusions

In this paper we have investigated the effect of an increasing dipole tilt angle on the global magnetosphere and its coupling with the solar wind and ionosphere, during a period of steady southward IMF. We find that the reconnection line on the magnetopause shifts southward with increasing tilt angle, in agreement with findings from previous studies. However, in extending the survey to larger angles than has previously been investigated we have revealed that the reconfiguration of the magnetic separator is complex and time dependent, especially for larger tilt angles. Even for a 90° tilt angle, the separator is continuous across the entire dayside magnetopause, and reconnection appears active along its extent.

The magnetosphere is thus still "open" for an arbitrarily large tilt angle, with the reconnection voltage dropping (above 10°) with increasing tilt angle and the polar cap contracting. We find that a 0° tilt angle presents a unique case compared to nonzero angles, as the strong antisymmetry in the system renders both dayside and nightside reconnection to be less stable than at 10° and show a more complex time dependence. We emphasize that steady state represents a special case and that a more smooth trend in dayside reconnection voltage may be seen if driving with a varying IMF, rather than with the steady conditions for several hours. However, this would introduce more complex responses in the global system such that the effect of the dipole tilt angle alone would be hard to diagnose.

The reduced geoeffectiveness at large tilt angles may be a result of strongly diverted magnetosheath flow where the separator is offset far from the subsolar region. Reconnection is also increasingly unsteady as the tilt angle becomes large, with FTE generation becoming more persistent, thus making the rate of flux transfer highly time dependent. This appears to be associated with an offset of the magnetosheath flow stagnation point from the separator location. Away from noon, the separator is more steady, but the reconnection rate is generally lower due to reduced magnetic shear angle. This has implications for reconnection at magnetospheres with highly inclined dipoles, for example, at the ice giants where observations are extremely limited. For example, it has been shown that seasonal modulation in magnetic shear angle at Neptune's magnetopause is likely to strongly alter where reconnection occurs (Masters, 2015), while simulations reveal that reconnection can locally "switch-off" for certain periods of planetary rotation (e.g., Cao & Paty, 2017; Mejnertsen et al., 2016). An investigation into the separator location for the various extreme configurations of the ice giant magnetospheres could thus reveal to what extent reconnection can be globally active even where the shear angle is small, and whether it is strongly FTE-driven.

In our terrestrial context the drop in reconnection voltage is associated with a contracting ionospheric polar cap, and shrinking region I current systems and CPCPs. However, the strength of these currents shows a more nonlinear dependence on tilt angle. We have shown that as the tilt angle increases, an asymmetry between the convection path lengths of northern and southern open magnetospheric field lines emerges. In order to sustain a steady state, northern ionospheric currents can thus reach larger intensities than their southern counterparts, despite equal polar cap flux content, and the CPCP becomes larger in the north even without including conductance changes. The morphology of these currents also begins to vary significantly, showing a bias on the dayside in the north but more day-night symmetry in the south. While this static configuration does not reflect a realistic scenario for the terrestrial magnetosphere (since dipole rotation and nonuniform conductance will act to smooth out some of the asymmetry over hours), the existence of this asymmetry has implications for the potential impact of a severe space weather event. For example, at the onset of a geomagnetic storm, the hemisphere which preferentially faces the solar wind may experience more intense and/or localized FAC (and thus ground magnetic perturbations) close to solstice and affect sudden storm commencements (see Eastwood et al., 2018, and references therein) even despite any differences in conductance.

It is important to point out that migration of the geomagnetic poles over geological timescales would remap the ionospheric coordinates onto lower geographic latitudes. The severe tilt angle cases presented here thus reveal that in this scenario, lower-latitude regions may become susceptible to increasingly significant space weather impacts, but constrained to a smaller polar cap region. Furthermore, periods of geomagnetic reversal are associated with changes in the strength of the Earth's dipole moment, which will give rise to additional changes in ionospheric coupling (e.g., Cnossen, Richmond, & Wiltberger, 2012). Our study could thus be extended further to explore how various changes in the internal magnetic field affect the impact of a given severe event.

Finally, there are a number of caveats in our study that could be addressed in future investigations. The inclusion of a high-resolution magnetopause and a more physics-based resistivity would allow more detailed investigation into the local behavior along the separator, rather than just its global configuration. Extending the model to include Hall-MHD would directly affect the local reconnection rate via the Hall electric field, and it is not known if this affects the location of the separator. Exploring various additional IMF orientations may reveal further complex dependencies on the tilt angle, as has previously been done in the case of a 15° tilt angle and 30° IMF clock angle (Komar et al., 2015). For example, by breaking the antisymmetry between the IMF and magnetospheric field in the 0° case, a different trend from 0–10° could be seen. While these additional factors are all fundamental and help to build the overall picture, the study presented here demonstrates that the underlying trend driven by the dipole tilt alone has a significant impact on the global magnetosphere-ionosphere system, which varies strongly over the full range of tilt angles.

Data Availability Statement

The simulation data used in this paper are openly available on the Centre for Environmental Data Analysis (CEDA) (doi:10.5285/77d63a69e3554412a40c9a9ba564e3f9).

Acknowledgments

J. W. B. E. is funded by a UK Science and Technology Facilities Council (STFC) Studentship (ST/R504816/1). Research into magnetospheric modeling at ICL is also supported by National Environment Research Council (NERC) Grants NE/P017142/1 (SWIGS) and NE/P017347/1 (Rad-Sat). This work used the Imperial College High Performance Computing Service (doi: 10.14469/hpc/2232). The authors would like to thank the anonymous reviewers for their insightful comments, which provided valuable input into this article.

References

Amit, H., & Olson, P. (2008). Geomagnetic dipole tilt changes induced by core flow. *Physics of the Earth and Planetary Interiors*, *166*(3-4), 226–238. https://doi.org/10.1016/j.pepi.2008.01.007

Cao, X., & Paty, C. (2017). Diurnal and seasonal variability of Uranus's magnetosphere. *Journal of Geophysical Research: Space Physics*, *122*, 6318–6331. https://doi.org/10.1002/2017JA024063

Cassak, P. A., & Fuselier, S. A. (2016). Reconnection at Earth's dayside magnetopause. In W. Gonzalez, & E. Parker (Eds.), *Magnetic Reconnection. Astrophysics and Space Science Library* (Vol. 427, pp. 213–276). Cham: Springer.

Ciardi, A., Lebedev, S. V., Frank, A., Blackman, E. G., Chittenden, J. P., Jennings, C. J., et al. (2007). The evolution of magnetic tower jets in the laboratory. *Physics of Plasmas*, *14*(5), 056501. https://doi.org/10.1063/1.2436479

Cnossen, I., & Richmond, A. D. (2012). How changes in the tilt angle of the geomagnetic dipole affect the coupled magnetosphere-ionosphere-thermosphere system. *Journal of Geophysical Research*, *117*, A10317. https://doi.org/10.1029/2012JA018056

Cnossen, I., Richmond, A. D., & Wiltberger, M. (2012). The dependence of the coupled magnetosphere-ionosphere-thermosphere system on the Earth's magnetic dipole moment. *Journal of Geophysical Research*, *117*, A05302. https://doi.org/10.1029/2012JA017555

Cnossen, I., Wiltberger, M., & Ouellette, J. E. (2012). The effects of seasonal and diurnal variations in the Earth's magnetic dipole orientation on solar wind-magnetosphere-ionosphere coupling. *Journal of Geophysical Research*, *117*, A11211. https://doi.org/10.1029/2012JA017825

Cowley, S. W. H. (2000). Magnetosphere-Ionosphere Interactions: A tutorial review.In S. Ohtani (Ed.), *Magnetospheric current systems*, *Geophysical Monograph Series* (Vol. 118, pp. 91–106). Washington, DC: American Geophysical Union. https://doi.org/10.1029/GM118p0091

Cowley, S. W. H. (2013). Response of Uranus' auroras to solar wind compressions at equinox. *Journal of Geophysical Research: Space Physics*, *118*, 2897–2902. https://doi.org/10.1002/jgra.50323

Coxon, J. C., Milan, S. E., Carter, J. A., Clausen, L. B. N., Anderson, B. J., & Korth, H. (2016). Seasonal and diurnal variations in AMPERE observations of the Birkeland currents compared to modeled results. *Journal of Geophysical Research: Space Physics*, *121*, 4027–4040. https://doi.org/10.1002/2015JA022050

Crooker, N. U. (1979). Dayside merging and cusp geometry. *Journal of Geophysical Research*, *84*(A3), 951–959. https://doi.org/10.1029/JA084iA03p00951

Dorelli, J. C., & Bhattacharjee, A. (2009). On the generation and topology of flux transfer events. *Journal of Geophysical Research*, *114*, A06213. https://doi.org/10.1029/2008JA013410

Dungey, J. W. (1961). Interplanetary magnetic field and the auroral zones. *Physical Review Letters*, *6*(2), 47–48. https://doi.org/10.1103/PhysRevLett.6.47

Dunlop, M. W., Zhang, Q. H., Bogdanova, Y. V., Lockwood, M., Pu, Z., Hasegawa, H., et al. (2011). Extended magnetic reconnection across the dayside magnetopause. *Physical Review Letters*, *107*(2), 1–6. https://doi.org/10.1103/PhysRevLett.107.025004

Dunlop, M. W., Zhang, Q. H., Bogdanova, Y. V., Trattner, K. J., Pu, Z., Hasegawa, H., et al. (2011). Magnetopause reconnection across wide local time. *Annales Geophysicae*, *29*(9), 1693–1697. https://doi.org/10.5194/angeo-29-1683-2011

Eastwood, J. P., Hapgood, M. A., Biffis, E., Benedetti, D., Bisi, M. M., Green, L., et al. (2018). Quantifying the economic value of space weather forecasting for power grids: An exploratory study. *Space Weather*, *16*, 2052–2067. https://doi.org/10.1029/2018SW002003

Eastwood, J. P., Nakamura, R., Turc, L., Mejnertsen, L., & Hesse, M. (2017). The scientific foundations of forecasting magnetospheric space weather. *Space Science Reviews*, *212*(3-4), 1221–1252. https://doi.org/10.1007/s11214-017-0399-8

Eastwood, J. P., Phan, T. D., Øieroset, M., Shay, M. A., Malakit, K., Swisdak, M., et al. (2013). Influence of asymmetries and guide fields on the magnetic reconnection diffusion region in collisionless space plasmas. *Plasma Physics and Controlled Fusion*, *55*(12), 124001. https://doi.org/10.1088/0741-3335/55/12/124001

Eggington, J. W. B., Eastwood, J. P., Mejnertsen, L., Desai, R. T., & Chittenden, J. P. (2018). Forging links in Earth's plasma environment. *Astronomy & Geophysics*, *59*(6), 6.26–6.28. https://doi.org/10.1093/astrogeo/aty275

Glocer, A., Dorelli, J., Toth, G., Komar, C. M., & Cassak, P. A. (2016). Separator reconnection at the magnetopause for predominantly northward and southward IMF: Techniques and results. *Journal of Geophysical Research: Space Physics*, *121*, 140–156. https://doi.org/10.1002/2015JA021417

Gonzalez, W. D., & Mozer, F. S. (1974). A quantitative model for the potential resulting from reconnection with an arbitrary interplanetary magnetic field. *Journal of Geophysical Research*, *79*(28), 4186–4194. https://doi.org/10.1029/JA079i028p04186

Goodman, M. L. (1995). A three-dimensional, iterative mapping procedure for the implementation of an ionosphere-magnetosphere anisotropic Ohm's law boundary condition in global magnetohydrodynamic simulations. *Annales Geophysicae*, *13*(8), 843–853. https://doi.org/10.1007/s00585-995-0843-z

Grießmeier, J.-M., Stadelmann, A., Penz, T., Lammer, H., Selsis, F., Ribas, I., et al. (2004). The effect of tidal locking on the magnetospheric and atmospheric evolution of Hot Jupiters. *Astronomy & Astrophysics*, *425*(2), 753–762. https://doi.org/10.1051/0004-6361:20035684

Gubbins, D. (2008). Earth science: Geomagnetic reversals. *Nature*, *452*, 165–167. https://doi.org/10.1038/452165a

Hapgood, M. A. (1992). Space physics coordinate transformations: A user guide. *Planetary and Space Science*, *40*(5), 711–717. https://doi.org/10.1016/0032-0633(92)90012-D

Haynes, A. L., & Parnell, C. E. (2007). A trilinear method for finding null points in a three-dimensional vector space. *Physics of Plasmas*, *14*(8), 082107. https://doi.org/10.1063/1.2756751

Hesse, M. (1997). On the mapping of ionospheric convection into the magnetosphere. *Journal of Geophysical Research*, *102*(A5), 9543–9551. https://doi.org/10.1029/96JA03999

Hesse, M., Neukirch, T., Schindler, K., Kuznetsova, M., & Zenitani, S. (2011). The diffusion region in collisionless magnetic reconnection. *Space Science Reviews*, *160*, 3–23. https://doi.org/10.1007/s11214-010-9740-1

Hoilijoki, S., Souza, V. M., Walsh, B. M., Janhunen, P., & Palmroth, M. (2014). Magnetopause reconnection and energy conversion as influenced by the dipole tilt and the IMF Bx. *Journal of Geophysical Research: Space Physics*, *119*, 4484–4494. https://doi.org/10.1002/2013JA019693

Hoppe, H., DeRose, T., Duchamp, T., McDonald, J., & Stuetzle, W. (1992). Surface reconstruction from unorganized points. *SIGGRAPH Comput. Graph.*, *26*(2), 71–78. https://doi.org/10.1145/142920.134011

Hoshi, Y., Hasegawa, H., Kitamura, N., Saito, Y., & Angelopoulos, V. (2018). Seasonal and solar wind control of the reconnection line location on the Earth's dayside magnetopause. *Journal of Geophysical Research: Space Physics*, *123*, 7498–7512. https://doi.org/10.1029/2018JA025305

Jelínek, K., Němeček, Z., Šafránková, J., & Merka, J. (2008). Influence of the tilt angle on the bow shock shape and location. *Journal of Geophysical Research*, *113*, A05220. https://doi.org/10.1029/2007JA012813

Komar, C. M., Cassak, P. A., Dorelli, J. C., Glocer, A., & Kuznetsova, M. M. (2013). Tracing magnetic separators and their dependence on IMF clock angle in global magnetospheric simulations. *Journal of Geophysical Research: Space Physics*, *118*, 4998–5007. https://doi.org/10.1002/jgra.50479

Komar, C. M., Fermo, R. L., & Cassak, P. A. (2015). Comparative analysis of dayside magnetic reconnection models in global magnetosphere simulations. *Journal of Geophysical Research: Space Physics*, *120*, 276–294. https://doi.org/10.1002/2014JA020587

Korte, M., & Mandea, M. (2008). Magnetic poles and dipole tilt variation over the past decades to millennia. *Earth, Planets and Space*, *60*(9), 937–948. https://doi.org/10.1186/BF03352849

Liu, Z.-Q., Lu, J. Y., Kabin, K., Yang, Y. F., Zhao, M. X., & Cao, X. (2012). Dipole tilt control of the magnetopause for southward IMF from global magnetohydrodynamic simulations. *Journal of Geophysical Research*, *117*, A07207. https://doi.org/10.1029/2011JA017441

Lu, J. Y., Liu, Z.-Q., Kabin, K., Jing, H., Zhao, M. X., & Wang, Y. (2013). The IMF dependence of the magnetopause from global MHD simulations. *Journal of Geophysical Research: Space Physics*, *118*, 3113–3125. https://doi.org/10.1002/jgra.50324

Lu, J. Y., Zhang, H., Wang, M., Gu, C., & Guan, H. (2019). Magnetosphere response to the IMF turning from north to south. *Earth and Planetary Physics*, *3*(1), 8–16. https://doi.org/10.26464/epp2019002

Lu, J. Y., Zhou, Y., Ma, X., Wang, M., Kabin, K., & Yuan, H. Z. (2019). Earth's bow shock: A new three dimensional asymmetric model with dipole tilt effects. *Journal of Geophysical Research: Space Physics*, *124*, 5396–5407. https://doi.org/10.1029/2018JA026144

Masters, A. (2015). Magnetic reconnection at Neptune's magnetopause. *Journal of Geophysical Research: Space Physics*, *120*, 479–493. https://doi.org/10.1002/2014JA020744

Mejnertsen, L. (2018). The dynamics of the outer boundaries in global simulations of planetary magnetospheres. (PhD thesis). Imperial College London. https://doi.org/10.25560/65696

Mejnertsen, L., Eastwood, J. P., Chittenden, J. P., & Masters, A. (2016). Global MHD simulations of Neptune's magnetosphere. *Journal of Geophysical Research: Space Physics*, *121*, 7497–7513. https://doi.org/10.1002/2015JA022272

Mejnertsen, L., Eastwood, J. P., Hietala, H., Schwartz, S. J., & Chittenden, J. P. (2018). Global MHD simulations of the Earth's bow shock shape and motion under variable solar wind conditions. *Journal of Geophysical Research: Space Physics*, *123*, 259–271. https://doi.org/10.1002/2017JA024690

Merkin, V. G., & Lyon, J. G. (2010). Effects of the low-latitude ionospheric boundary condition on the global magnetosphere. *Journal of Geophysical Research*, *115*, A02208. https://doi.org/10.1029/2009JA014212

Merkin, V. G., Papadopoulos, K., Milikh, G., Sharma, A. S., Shao, X., Lyon, J., & Goodrich, C. (2003). Effects of the solar wind electric field and ionospheric conductance on the cross polar cap potential: Results of global MHD modeling. *Geophysical Research Letters*, *30*(23), 2180. https://doi.org/10.1029/2003GL017903

Palmroth, M., Pulkkinen, T. I., Janhunen, P., & Wu, C. C. (2003). Stormtime energy transfer in global MHD simulation. *Journal of Geophysical Research*, *108*(A1), 1048. https://doi.org/10.1029/2002JA009446

Papitashvili, V. O., Christiansen, F., & Neubert, T. (2002). A new model of field-aligned currents derived from high-precision satellite magnetic field data. *Geophysical Research Letters*, *29*(14), 28-1–28-4. https://doi.org/10.1029/2001GL014207

Park, K. S., Ogino, T., & Kim, Y. H. (2010). Effects of the dipole tilt and northward and duskward IMF on dayside magnetic reconnection in a global MHD simulation. *Journal of Geophysical Research*, *115*, A02208. https://doi.org/10.1029/2009JA014212

Park, K. S., Ogino, T., & Walker, R. J. (2006). On the importance of antiparallel reconnection when the dipole tilt and IMF By are nonzero. *Journal of Geophysical Research*, *111*, A05202. https://doi.org/10.1029/2004JA010972

Paschmann, G., Øieroset, M., & Phan, T. (2013). In-situ observations of reconnection in space. *Space Science Reviews*, *178*(2-4), 385–417. https://doi.org/10.1007/s11214-012-9957-2

Peng, Z., Wang, C., & Hu, Y. Q. (2010). Role of IMF B_x in the solar wind-magnetosphere-ionosphere coupling. *Journal of Geophysical Research*, *115*, A08224. https://doi.org/10.1029/2010JA015454

Pettigrew, E. D., Shepherd, S. G., & Ruohoniemi, J. M. (2010). Climatological patterns of high-latitude convection in the Northern and Southern Hemispheres: Dipole tilt dependencies and interhemispheric comparisons. *Journal of Geophysical Research*, *115*, A07305. https://doi.org/10.1029/2009JA014956

Raeder, J. (2006). Flux transfer events: 1. Generation mechanism for strong southward IMF. *Annales Geophysicae*, *24*(1), 381–392. https://doi.org/10.5194/angeo-24-381-2006

Ridley, A. J. (2007). Effects of seasonal changes in the ionospheric conductances on magnetospheric field-aligned currents. *Geophysical Research Letters*, *34*, L05101. https://doi.org/10.1029/2006GL028444

Ridley, A. J., Gombosi, T. I., & Dezeeuw, D. L. (2004). Ionospheric control of the magnetosphere: Conductance. *Annales Geophysicae*, *22*(2), 567–584. https://doi.org/10.5194/angeo-22-567-2004

Ridley, A. J., Gombosi, T. I., Sokolov, I. V., Tóth, G., & Welling, D. T. (2010). Numerical considerations in simulating the global magnetosphere. *Annales Geophysicae*, *28*(8), 1589–1614. https://doi.org/10.5194/angeo-28-1589-2010

Russell, C. T., & Dougherty, M. K. (2010). Magnetic fields of the outer planets. *Space Science Reviews*, *152*(1-4), 251–269. https://doi.org/10.1007/s11214-009-9621-7

Russell, C. T., & McPherron, R. L. (1973). Semiannual variation of geomagnetic activity. *Journal of Geophysical Research*, *78*(1), 92–108. https://doi.org/10.1029/JA078i001p00092

Russell, C. T., Wang, Y. L., & Raeder, J. (2003). Possible dipole tilt dependence of dayside magnetopause reconnection. *Geophysical Research Letters*, *30*(18), 1937. https://doi.org/10.1029/2003GL017725

Sonnerup, B. U. O. (1974). Magnetopause reconnection rate. *Journal of Geophysical Research*, *79*(10), 1546–1549. https://doi.org/10.1029/JA079i010p01546

Souza, V. M., Gonzalez, W. D., Sibeck, D. G., Koga, D., Walsh, B. M., & Mendes, O. (2017). Comparative study of three reconnection X line models at the Earth's dayside magnetopause using in situ observations. *Journal of Geophysical Research: Space Physics*, *122*, 4228–4250. https://doi.org/10.1002/2016JA023790

Tanaka, T. (1994). Finite volume TVD scheme on an unstructured grid system for three-dimensional mhd simulation of inhomogeneous systems including strong background potential fields. *Journal of Computational Physics*, *111*(2), 381–389. https://doi.org/10.1006/JCPH.1994.1071

Trattner, K. J., Mulcock, J. S., Petrinec, S. M., & Fuselier, S. A. (2007). Probing the boundary between antiparallel and component reconnection during southward interplanetary magnetic field conditions. *Journal of Geophysical Research*, *112*, A08210. https://doi.org/10.1029/2007JA012270

Trattner, K. J., Petrinec, S. M., Fuselier, S. A., & Phan, T. D. (2012). The location of reconnection at the magnetopause: Testing the maximum magnetic shear model with THEMIS observations. *Journal of Geophysical Research*, *117*, A01201. https://doi.org/10.1029/2011JA016959

Uzdensky, D. A. (2003). Petschek-like reconnection with current-driven anomalous resistivity and its application to solar flares. *The Astrophysical Journal*, *587*(1), 450–457. https://doi.org/10.1086/368075

van der Walt, S., Schönberger, J. L., Nunez-Iglesias, J., Boulogne, F., Warner, J. D., Yager, N., et al. (2014). Scikit-image: Image processing in Python. *PeerJ*, *2*, e453. https://doi.org/10.7717/peerj.453

Walsh, B. M., Komar, C. M., & Pfau-Kempf, Y. (2017). Spacecraft measurements constraining the spatial extent of a magnetopause reconnection X line. *Geophysical Research Letters*, *44*, 3038–3046. https://doi.org/10.1002/2017GL073379

Wang, H., Lühr, H., & Ma, S. Y. (2005). Solar zenith angle and merging electric field control of field-aligned currents: A statistical study of the Southern Hemisphere. *Journal of Geophysical Research*, *110*, A03306. https://doi.org/10.1029/2004JA010530

Xiao, S., Zhang, T., Ge, Y., Wang, G., Baumjohann, W., & Nakamura, R. (2016). A statistical study on the shape and position of the magnetotail neutral sheet. *Annales Geophysicae*, *34*(2), 303–311. https://doi.org/10.5194/angeo-34-303-2016

Yeh, T. (1976). Day side reconnection between a dipolar geomagnetic field and a uniform interplanetary field. *Journal of Geophysical Research*, *81*(13), 2140–2144. https://doi.org/10.1029/JA081i013p02140

Zhang, S.-R., Holt, J. M., & McCready, M. (2007). High latitude convection based on long-term incoherent scatter radar observations in North America. *Journal of Atmospheric and Solar-Terrestrial Physics*, *69*(10-11), 1273–1291. https://doi.org/10.1016/J.JASTP.2006.08.017

Zhu, C. B., Zhang, H., Ge, Y. S., Pu, Z. Y., Liu, W. L., Wan, W. X., et al. (2015). Dipole tilt angle effect on magnetic reconnection locations on the magnetopause. *Journal of Geophysical Research: Space Physics*, *120*, 5344–5354. https://doi.org/10.1002/2015JA020989